Available online at www.sciencedirect.com
SCIENCE DIRECT®
PERGAMON
Applied Geochemistry 18 (2003) 1705–1721
Applied Geochemistry
www.elsevier.com/locate/apgeochem

Characterization of limestone reacted with acid-mine drainage in a pulsed limestone bed treatment system at the Friendship Hill National Historical Site, Pennsylvania, USA

Jane M. Hammarstrom[a,*], Philip L. Sibrell[b], Harvey E. Belkin[a]

[a]US Geological Survey, 954 National Center, Reston, VA 20192, USA
[b]US Geological Survey, Leetown Science Center, 11700 Leetown Road, Kearneysville, WV 25430, USA

Received 12 August 2002; accepted 15 May 2003
Editorial handling by B.A. Kimball

Abstract

Armoring of limestone is a common cause of failure in limestone-based acid-mine drainage (AMD) treatment systems. Limestone is the least expensive material available for acid neutralization, but is not typically recommended for highly acidic, Fe-rich waters due to armoring with Fe(III) oxyhydroxide coatings. A new AMD treatment technology that uses CO_2 in a pulsed limestone bed reactor minimizes armor formation and enhances limestone reaction with AMD. Limestone was characterized before and after treatment with constant flow and with the new pulsed limestone bed process using AMD from an inactive coal mine in Pennsylvania (pH = 2.9, Fe = 150 mg/l, acidity = 1000 mg/l $CaCO_3$). In constant flow experiments, limestone is completely armored with reddish-colored ochre within 48 h of contact in a fluidized bed reactor. Effluent pH initially increased from the inflow pH of 2.9 to over 7, but then decreased to <4 during the 48 h of contact. Limestone grains developed a rind of gypsum encapsulated by a 10- to 30-μm thick, Fe-Al hydroxysulfate coating. Armoring slowed the reaction and prevented the limestone from generating any additional alkalinity in the system. With the pulsed flow limestone bed process, armor formation is largely suppressed and most limestone grains completely dissolve resulting in an effluent pH of >6 during operation. Limestone removed from a pulsed bed pilot plant is a mixture of unarmored, rounded and etched limestone grains and partially armored limestone and refractory mineral grains (dolomite, pyrite). The ~30% of the residual grains in the pulsed flow reactor that are armored have thicker (50- to 100-μm), more aluminous coatings and lack the gypsum rind that develops in the constant flow experiment. Aluminium-rich zones developed in the interior parts of armor rims in both the constant flow and pulsed limestone bed experiments in response to pH changes at the solid/solution interface.

1. Introduction

Acid-mine drainage (AMD) is an unintended consequence of coal and metal mining that adversely affects thousand of kilometers of streams in the United States. Estimated costs of remediation for the state of Pennsylvania alone using current technology range upwards of 5 billion dollars (US Environmental Protection Agency, 2000). More economical treatment methods are needed to address this issue with the limited resources available. A novel low-cost AMD treatment process based on limestone neutralization has been developed and patented at the US Geological Survey Leetown Science Center in Kearneysville, West Virginia (Watten, 1999). Limestone is the most cost effective neutralization material available, but has not been used widely for

* Corresponding author. Tel.: 1-703-648-6165; fax: 1-703-648-6252.
E-mail address: jhammars@usgs.gov (J.M. Hammarstrom).

0883-2927/03/$ - see front matter © 2003 Elsevier Ltd. All rights reserved.
doi:10.1016/S0883-2927(03)00105-7

neutralization of AMD because of its slow rate of dissolution and tendency for an impermeable metal-hydroxide coating, termed armoring, to form on grain surfaces. Limestone is not recommended for sites with acidity levels greater than 50 mg/l as $CaCO_3$ or Fe concentrations above 5 mg/l because of armoring (Skousen et al., 1995). The new process overcomes these problems through addition of CO_2 to the AMD to increase limestone dissolution rate, and through pulsed fluidized beds, causing particle–particle abrasion, thus scouring the limestone surface and abrading any coatings that form. The high water velocity in the fluidized beds also flushes precipitates out of the system, preventing plugging problems that can occur with packed limestone beds. The process has been successfully field tested at several sites (Sibrell et al., 2000) with moderate acidity (300 mg/l $CaCO_3$) and Fe (30 mg/l) levels.

The effectiveness of the pulsed bed process at higher acidities and Fe levels was tested at the National Park Service's Friendship Hill National Historic Site, south of Pittsburgh, Pennsylvania. AMD containing about 1000 mg/l $CaCO_3$ acidity and 150 mg/l Fe flows from an abandoned coal mine through park property to the Monongahela River. Based on data compiled by Rose and Cravotta (1998), this drainage has higher acid and metal concentrations than 90% of AMD drainages in the state of Pennsylvania. A limestone compost wetland had been tested earlier at this site, but had failed because of the excessive Fe and acidity levels (Hedin et al., 1994). AMD at the site in the fall of 2000 (Table 1) had a pH of 2.9, an acidity of 974 mg/l $CaCO_3$, and a Fe concentration of 167 mg/l. A pilot plant capable of treating up to 227 l/min of AMD was constructed at the Friendship Hill site during 1999–2000. The process includes treatment of the water in a pulsed limestone bed, followed by air stripping to remove CO_2 generated by reaction of limestone with AMD. Some of the CO_2 is recovered and recycled to the incoming AMD through the use of perforated tray scrubber towers. Settling tanks remove metal hydroxide solids from the treated water, and then the water is pumped back to the stream headwaters. At Friendship Hill, the influent acidity was sufficient to generate CO_2 so that no addition of commercial CO_2 was required. Plant testing began on a continuous basis in July 2000, and ran through September 2001. Table 1 also shows analysis of the plant effluent leaving the settling tanks. The effluent is at a neutral pH, with net alkalinity. The removal efficiencies were 95% for acidity, 98% for Al, 75% for Fe, and less than 5% for Mn. Manganese requires higher pH (9.0–9.5) for removal. Iron removal is dependent on the concentration of the Fe(II), which varies throughout the year, from less than 2% in the spring to as much as 60% in the winter. The removal of Fe(II) is limited by the kinetics of oxidation to the Fe(III) state and subsequent hydrolysis. No inhibition of neutralization by armoring was observed in process effluent from the Friendship Hill pilot plant.

Table 1
AMD influent and pulsed bed reactor effluent at Friendship Hill on September 20, 2000[a]

Sample	Influent	Effluent
pH	2.9	6.5
T (°C)	14	14
Acidity (mg/l $CaCO_3$)	974	46
Alkalinity (mg/l $CaCO_3$)	0	64
Fe (mg/l)	167	42
Al (mg/l)	56	1.0
Mn (mg/l)	9.8	9.6
SO_4 (mg/l)	2200	2000

[a] Water analyses performed by Geochemical Testing, Somerset, PA.

Because prevention of armor coatings is essential for limestone-based neutralization processes, more information was needed to characterize the extent and nature of armor formation. A chemical and mineralogical study of the limestone feed material used at the Friendship Hill pilot plant was conducted. An experiment was also performed to investigate the behavior of the limestone when exposed to Friendship Hill AMD in a simple fluidized bed configuration without the pulsing process (i.e., constant flow). During the 48 h of the experiment, an obvious armor coating formed on the surface of the limestone grains. For comparison, a sample of the limestone that remained in the bottom of the reactor vessel after 3 months of pilot plant operation was also analysed. This paper discusses the chemistry and mineralogy of 3 limestone samples: (1) raw limestone feed material, (2) armored limestone from the 48-h constant flow experiment, and (3) limestone removed from the pulsed limestone bed reactor at the Friendship Hill pilot plant after 3 months of continuous operation.

2. Previous studies of armor formation

Several investigators have studied the effect of dissolved metals on AMD neutralization with limestone. Pearson and McDonnell (1975a) developed design models for the use of limestone in open channels for remediation of AMD. Several field installations were constructed based on these designs. After two years of operation, they found that an armor coating had developed on the limestone, reducing its effectiveness to 20% of fresh limestone. This factor was then introduced into the design procedure to account for the armoring (Pearson and McDonnell, 1975b). Ziemkiewicz et al. (1997) investigated the effect of armoring limestone on acid neutralization with limestone, and concluded that even after armoring, limestone was still partly effective in acid neutralization, but displayed a wide range of

inhibition, from 2 to 45% in a HCl acid solution. Cravotta and Trahan (1999) showed that limestone can be effective for AMD remediation in oxic limestone drains despite armoring by Fe and Al hydroxides.

A number of previous studies document the effects of armor coatings on limestone drain performance. Premature failure of oxic limestone drains due to armoring is well documented in the literature on treatment systems for coal mine drainage (Phipps et al., 1995). Anoxic limestone drains (ALDs) are commonly used to retard oxidation of soluble Fe(II) to Fe(III), which hydrolyzes and precipitates at a pH of about 3.5. For Al-rich AMD waters, white aluminous precipitates armor limestone under certain pH conditions. Dissolved Al in surface waters behaves conservatively at pH less than about 4.5–5.0. At higher pH, amorphous solids composed of Al-hydroxysulfate precipitate (Nordstrom and Alpers, 1999). Watzlaf et al. (2000) showed that ALDs that received 21 mg/l Al failed within 8 months of operation. In their study of ALDs, Robbins et al. (1999) suspended calcite slides at inflow and midstream points along several ALDs. Although they found that precipitates (ferrihydrite, schwertmannite, goethite, aluminite) and microbial populations were distinct for different locations, some of the calcite showed evidence of dissolution (pits and etch points) after 20 days of immersion. Gypsum crystals were observed with microbial filaments, suggesting microbial involvement in gypsum formation. In a drain clogged by a white precipitate, they concluded that calcite dissolution preceded aluminite precipitation because the aluminite coated etch points.

Few studies address the composition of armor coatings on limestone. In AMD neutralization applications, armor coatings can be composed of metal oxyhydroxides and hydroxysulfates or Ca sulfate (gypsum). Oxyhydroxides and gypsum may both precipitate in waters with high SO_4 and Ca content. Wentzler and Aplan (1972) studied the effects of SO_4 and Fe(III) using a rotating disk method, and found that inhibitory coatings were formed only in the range of pH 2–3, where $Fe(OH)^{++}$ is the predominant dissolved Fe species. These studies were conducted at high rotating speeds, so that ordinarily adherent coatings may have been sheared off the surface of the disk. Evangelou (1995) reported that $Fe(OH)_3$ precipitates are formed on the surface of limestone through adsorption of Fe(II), followed by oxidation to Fe(III). Limestone coatings at the Quakake Tunnel AMD treatment site in Pennsylvania were investigated by elemental analysis, X-ray diffraction and scanning electron microscopy (Geo-Technical Services, Inc., 1982). The influent AMD at this site is relatively mild: up to 110 mg/l $CaCO_3$ acidity, total Fe of less than 1 mg/l, and Al of up to 17 mg/l. The coatings were determined to take 3 forms: a porous recrystallized calcite, a brown, Fe-rich nonporous coating which flakes off when dry, and a nonporous flaking coating rich in Al and S. Loeppert and Hossner (1984) investigated the reaction of Fe(II) and Fe(III) perchlorate with calcite, which precipitated ferrihydrite and lepidocrocite (with air as the purge gas) or goethite (with CO_2). The precipitates did not suppress calcite dissolution rates in steady-state experiments at pH = 5.0 under stirred conditions. In most experiments, the rate of dissolution increased due to an increase in surface area from etching of calcite.

Societal concerns about the environmental effects of acid rain on weathering limestone buildings and monuments prompted research on the role of gypsum formation in passivating calcite surfaces to slow the weathering process. Booth et al. (1997) found that under certain conditions, the crystal lattices of calcite and gypsum that rapidly coats the calcite surface matched so that adherent growths were obtained. Channel flow cell studies by Wilkins et al. (2001) demonstrated that the formation of needles of gypsum crystallites on dissolving calcite surfaces reduces the rate of calcite dissolution by H_2SO_4; gypsum nuclei formed at edges and corners of calcite etch pits and over time, formed rosettes of flat platelets. The channel flow experiments showed that rate constants for calcite dissolution in 0.01 M H_2SO_4 decreased by an order of magnitude over 21 h of exposure (0.035–0.004 cm s^{-1}) due to passivation of the dissolving calcite surface by gypsum.

3. Experiments

Raw limestone sand used in the reactor at Friendship Hill was obtained from the Con Lime Limestone Company in Bellefonte, PA. This material is a high-Ca limestone mined from the Valentine Member of the Ordovician Linden Hall Formation in the Valley and Ridge province of central Pennsylvania (Berkheiser, 1985) and has a particle size distribution of about 20–100 mesh (0.86–0.14 mm).

The armored limestone sample was prepared in April 2000. Limestone sand was exposed to AMD at the Friendship Hill site for 48 h in a 10.2 cm diameter constant flow fluidized bed reactor. The flow rate of Friendship Hill AMD through the reactor was 2.6 l/min, resulting in a flow velocity of 0.5 cm s^{-1}. No CO_2 was added for this baseline test. The pH of the fluidized bed effluent was monitored as a function of time, and dropped from 7.5 at the beginning of the test to 3.3 after 48 h of operation, when the flow was stopped and a sample of the residual limestone, which consisted of completely armored, rounded grains, was removed.

The Friendship Hill pilot plant was operated continuously for 14 months from June of 2000 through August of 2001 using the pulsed limestone bed technology. The apparatus treated up to 227 l/min of AMD

using about 1089 kg (2400 pounds) of limestone contained in 4 fiberglass reactors each about 0.6 m in diameter and 2.1 m tall. During normal plant operation, incoming AMD was alternately directed on a 1-min cycle to 1 of 2 columns receiving and discharging water. The other two columns recirculated water, also on a 1-min cycle, through a packed bed gas absorption column, termed the carbonator, for additional treatment effect. Every 4 min, the treatment and receiving columns were switched. All flows were automatically controlled using electrically actuated ball valves controlled by a programmable timer. Each reactor contained 270 kg limestone and periodically received 227 l/min of AMD, resulting in an upwards water flow velocity of 1.3 cm/s. Limestone was consumed by reaction with acid at a rate dependent on the AMD flow and acidity. The reactor limestone sample was taken about 3 months after the plant startup, in October of 2000. At the time that the sample was taken, limestone consumption was 680 kg per week, which was replenished by biweekly addition of fresh limestone to each reactor. Therefore, particles may have been in the reactor for as long as 3 months or as little as 4 days. Larger and heavier particles tend to remain in the reactor for a longer time, due to their greater settling velocity. Due to chance, some limestone particles are retained in the reactors for a very short time, whereas others are retained for a longer time than average. Therefore, the reacted limestone sample is a complex mixture of particles with differing characteristics and histories. At the time the reactor sample was taken, the plant was operating normally, in that the pH of the treated water was 6.5 and the alkalinity was 64 mg/l $CaCO_3$. Table 1 shows the analysis of the unfiltered influent and effluent water at that time. Although not shown in Table 1, the Friendship Hill AMD influent also contained about 280 mg/l Ca, based on a later separate analysis.

4. Methods

4.1. Physical and chemical methods

Mineral solids from the experiments were air dried and processed for analysis. Samples were examined under a binocular microscope and photographed. The bulk chemistry of samples of raw limestone, armored limestone, and reactor limestone was determined by X-ray fluorescence methods by Bondar-Clegg, Sparks, NV. Sulfate (reported as SO_3) was determined by gravimetric methods, also by Bondar-Clegg. The surface areas of the raw limestone and the dried samples from the experiments were measured using Kr or N_2 gas absorption and calculated by the BET method (any use of trade, product, or firm names is for descriptive purposes only and does not imply endorsement by the US Government); BET analyses were performed by the Micromeritics Instrument Corporation and the Materials Characterization Laboratory at Pennsylvania State University. Nitrogen is the gas normally used for measuring surface areas, but Kr should be used for samples with low specific surface area (Webb and Orr, 1997).

4.2. Scanning electron microscopy (SEM)

A JEOL JSM-840 scanning electron microscope equipped with a back-scattered electron (BSE) detector and a secondary electron (SEI) detector was used to examine armor thickness, document textures, and obtain qualitative information on composition using a PGT X-ray energy dispersive system (EDS). Armored limestone grains were shaken by mechanical sieving and examined under a binocular microscope to select intact grains that showed layer stages of development of the armor coating. Grains were placed on sticky C tape on a glass slide and C-coated. The SEM was operated at a voltage of 15 kV. Scale bars on SEI images are shown in μm.

4.3. X-ray diffraction (XRD)

Minerals were identified by powder XRD using a Scintag X1 automated powder diffractometer equipped with a Peltier detector with CuK_α radiation. Samples of the raw limestone sand, the armored limestone, and the reactor limestone were milled in acetone for 3 min using a micronizer. Air-dried powders were mounted in side-loading Al holders. Step scans were run over the range 5–70° 2-θ, with 0.02° stepping intervals and 0.5 s count time. Patterns were interpreted with the aid of Scintag and MDI Applications JADE search/match software and compared with standard reference patterns (ICDD, 2000).

4.4. Electron microprobe analysis (EMPA)

Multiple grain mounts of each sample were prepared as polished sections for electron microprobe analysis. A JEOL JSX-8900 microprobe equipped with 5 wavelength-dispersive spectrometers was used to analyze mineral chemistry and zoning trends across limestone grains. The probe was operated at 12 kV with a beam current of 20 nanoamps. Natural and synthetic minerals were used as primary standards. The probe was operated in several modes: (1) SEM mode to acquire backscattered electron images, (2) quantitative point analyses of individual spots within grains, (3) point analysis traverses across grains using 20-μm step intervals, (4) elemental maps of entire grains, and (5) continuous traverses across grains for selected elements of interest.

4.5. Thermogravimetric analysis

Simultaneous thermogravimetric, evolved gas, and single differential thermal analyses were performed on samples of raw limestone (23.5 mg) and armored limestone (15.8 mg) using a Mettler TGA/SDTA851 thermal analyzer coupled to a Balzers benchtop quadrupole mass spectrometer (QMS). Samples were placed in 70-μl alumina crucibles and heated from 22 to 950 °C at 10 °C/min in an Ar atmosphere (50 ml/min). Evolved gases are transferred to the QMS via a 200 °C heated silica capillary and selected masses were monitored during the runs. Scans (ion current as a function of time) for individual masses of interest are plotted with the mass loss curves to document the nature of the thermal decomposition reactions.

4.6. Modal analysis

A sample of the limestone from the pulsed limestone bed reactor experiment was cemented to a glass slide with epoxy. Low-magnification (2.5×) photomicrographs were taken for 22 subareas of the slide, and every grain that could clearly be identified in the field of view was counted as an unarmored, partially armored, or completely armored grain to estimate the percentage of total residual grains that developed armor coatings. A total of 558 grains were counted.

5. Results

Three samples of limestone were analyzed for this study (Fig. 1). Coatings developed on essentially all of the limestone grains in the 48-h constant flow experiment; material removed from 1 of the fiberglass reactors after 3 months of operation of the pulsed limestone bed experiment is a mixture of fresh limestone, partially reacted limestone, and armored grains. Hereafter, these 2 samples are referred to as armored limestone and reactor limestone, respectively. Armor coatings were coherent when wet, but readily cracked and flaked off upon drying.

5.1. Raw limestone feed material

The limestone sand feed material is white to pale gray in color (Fig. 1) and most of the sand grains are angular. XRD patterns show that the dominant mineral is calcite, with a trace of quartz (Fig. 2). Pyrite inclusions as well as quartz and dolomite were found in polished grain mounts; no gypsum was detected. The bulk limestone feed material is Ca-rich (Table 2). The concentration of mineral impurities is less than 3% and CaO and loss-on-ignition figures are typical for limestone. The surface area of the limestone was measured as 0.32

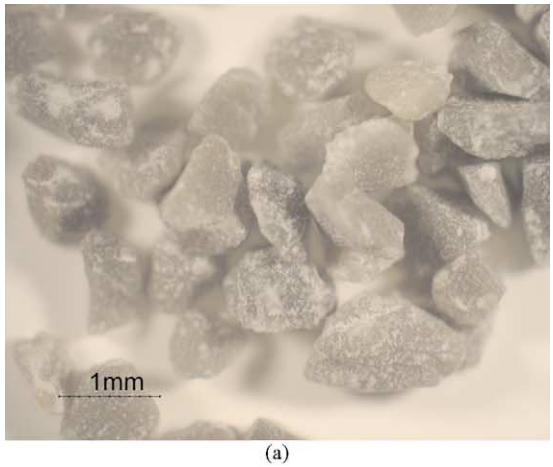

(a)

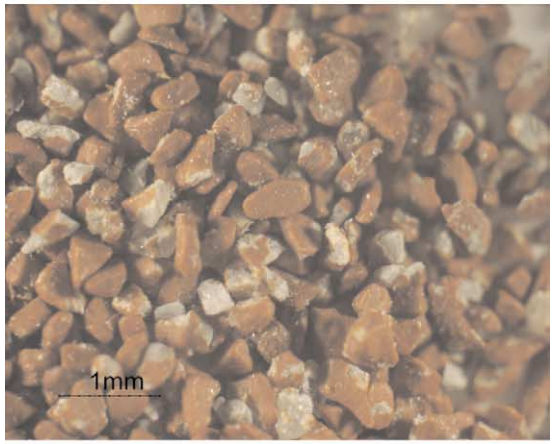

(b)

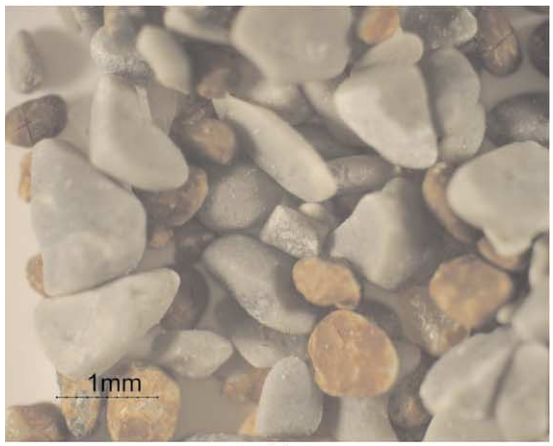

(c)

Fig. 1. Materials sampled for this study: (a) raw limestone sand; (b) armored limestone sampled after 48 h in the baseline experiment; (c) limestone removed from the Friendship Hill pulsed limestone bed reactor after 3 months.

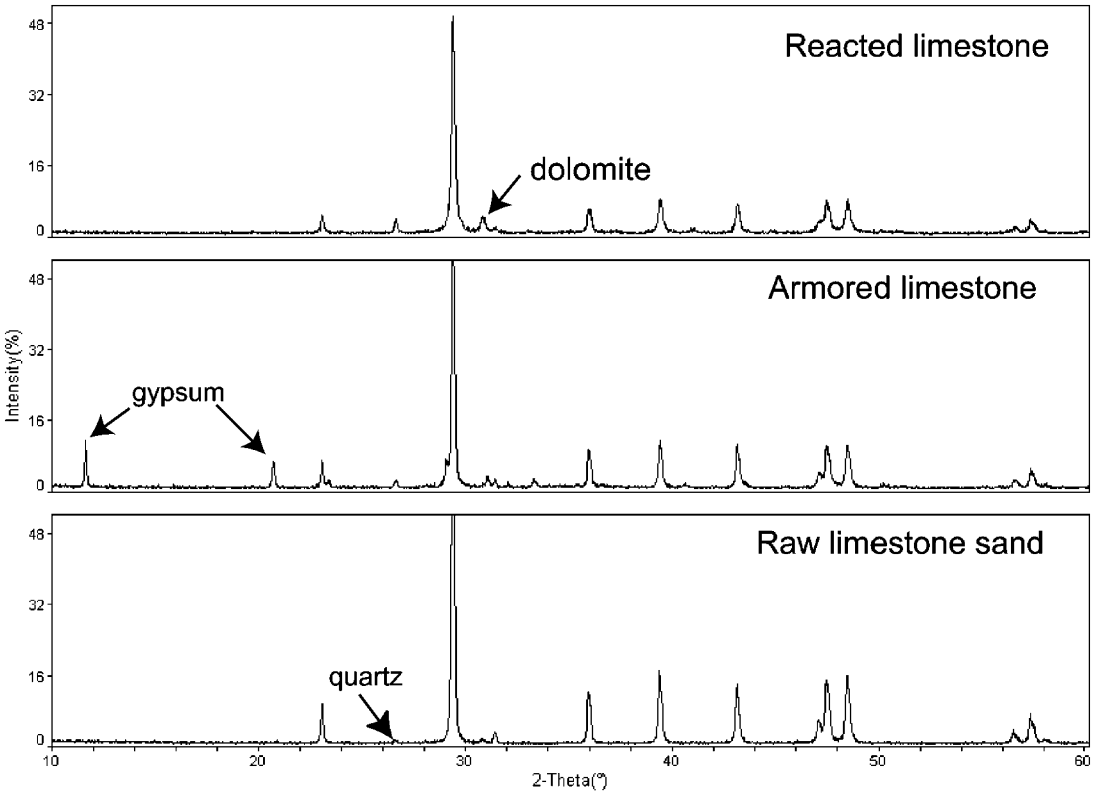

Fig. 2. X-ray powder diffraction patterns for raw limestone sand, armored limestone and reactor limestone. All unlabelled peaks match calcite, quartz, and dolomite.

Table 2
Bulk composition of limestone samples by X-ray fluorescence analysis (wt.%)

Sample	New limestone	Armored limestone from constant flow 48-h experiment	Limestone from the pulsed bed reactor
SiO_2	1.11	1.57	4.96
Al_2O_3	0.41	1.68	4.11
Fe_2O_3	0.12	10.04	3.83
MnO	<0.01	<0.01	<0.01
MgO	0.67	0.39	1.92
CaO	54.50	40.89	43.37
SO_3	0.00	5.94	0.75
LOI	42.85	36.87	39.04
Total	99.74	97.50	98.49

m^2/g by BET gas adsorption with Kr. The expected surface area for a non-porous spherical solid with the same particle size distribution as the limestone would be about 0.007 m^2/g. Shape factor effects could account for a doubling in surface area (Geiger and Poirier, 1973), but cannot explain orders-of-magnitude scale differences. Therefore, the limestone must have a pore structure that is accessible to Kr gas and that contributes to the surface area measurement. Limestone porosities typically range from <1 to 30%. Leith et al. (1996) observed a bimodal distribution of pore sizes in fossiliferous, high-Ca (97%) Salem limestone and reported the effective pore surface area as 1.51 m^2/g.

Microprobe data for the raw limestone are summarized in Table 3, along with data for limestone cores in armored limestone from the constant flow experiment. Nominal calcite composition is listed for reference. Water and CO_2 are not determined by microprobe, so totals are less than 100%. For the unaltered limestone, TGA/EGA analysis showed a mass loss of 43 wt.% at about 825 °C due to CO_2 loss (Fig. 3), which is in good agreement with the expected CO_2 content (44 wt.%) of ideal calcite. Fig. 4 shows secondary electron images of limestone surfaces from the 3 samples. The limestone sand grains have very rough surfaces (Fig. 4a), which is consistent with the high reported surface area.

5.2. Armored limestone

Essentially all of the limestone grains in the 48-h constant flow experiment became rounded and completely armored. When wet, the grains clump together and look like kidney beans. The armor coatings crack

Table 3
Microprobe data for limestone (wt.%)

	Unaltered limestone feed		Armored limestone cores		Natural calcite[a]
	Sample FH-LS		Sample FH-ALS		
	$n=36$		$n=18$		
	Avg	S.D.	Avg	S.D.	
FeO	0.04	0.05	0.17	0.10	0
SO_3	0.03	0.02	0.08	0.05	
Al_2O_3	0.07	0.15	0.19	0.27	
CuO	0.06	0.09	0.05	0.07	
ZnO	0.08	0.10	0.09	0.11	
MnO	0.01	0.02	0.01	0.02	Trace
MgO	0.27	0.11	0.44	0.14	0.04
CaO	54.2	2.0	55.0	1.7	55.92
K_2O	0.02	0.05	0.05	0.07	
Na_2O	0.03	0.02	0.03	0.02	
SiO_2	0.34	0.33	0.50	0.69	
CO_2[b]	43.0				43.95
Total	98.2	1.8	56.6	1.4	99.91

[a] Natural calcite composition from Deer et al. (1967).
[b] CO_2, determined from weight loss by thermogravimetry.

and flake as they dry, revealing cross-sections through the coatings. The bulk composition of the armored limestone (sample FH-ALS) shows increases in Fe, Al, and SO_4 contents, and a decrease in Ca content relative to the starting limestone bulk composition (Table 2). The significant increase in Fe content (0.12–10 wt.% total Fe reported as Fe_2O_3) reflects the composition of the armor coating. The bulk CaO content of the armored limestone sample is 41 wt.%, down from 54 wt.% of the raw limestone feed. Also, because some of that Ca is undoubtedly in the form of gypsum, the carbonate Ca is even less. In addition to dilution of the bulk composition by the armor components and attrition of limestone grains indicated by rounding, the chemical changes suggest that limestone was partly consumed in neutralization of AMD before armoring was complete.

Armored limestone grains are variable in size (Fig. 1), but typically measure up to 400 μm in diameter. The armor consists of thin layers (on the order of 10–30 micrometers) of dark reddish brown (Munsell 5YR 3/3) Fe ochre. A layer of gypsum is present between the limestone core and the ochre armor rim. The measured SO_3 content of the bulk armored limestone sample (Table 2), converted to gypsum, $CaSO_4{\cdot}2H_2O$, represents 12.8% of the sample weight. The gypsum forms a relatively continuous inner rim; gypsum grows as radiating sprays of crystals (Fig. 5b). The outermost armor shell appears smooth under low magnification (Fig. 5c). High magnification (Fig. 5d at 5000×) on the SEM shows that the armor consists of micrometer-scale rounded grains, with no definitive crystal morphology. EDS spectra (Fig. 6) show peaks for Ca and S that are consistent with the morphology and XRD identification of gypsum. EDS spectra also show that the remaining limestone core is essentially pure $CaCO_3$, and that the armor coatings are variable in composition especially with respect to Al and Fe. Innermost armor coatings are Al-rich relative to the outermost coatings and Si is detected in minor to trace amounts throughout the armor. No discrete crystals of quartz were identified in the armor.

No Fe mineral phase was identified by powder X-ray diffraction on armored grains, but gypsum is detected along with a trace of quartz. Many Fe oxyhydroxide (ferrihydrite) and Fe hydroxysulfate (schwertmannite) minerals encountered in acid-mine drainage are very poorly crystalline phases (Bigham, 1994). Typically, these phases are amorphous by XRD or produce broad, diffuse humps instead of sharp peaks. In addition, mineral phases that comprise less than 5 wt.% of a sample may not always be detected, especially when the material is poorly crystalline. The slightly lower peak to noise ratio of the armored limestone pattern is consistent with the presence of Fe-rich amorphous material.

Microprobe data for the armor coatings are listed in Table 4. Compositional trends across armored grains are illustrated in Fig. 7. Oxidation states of Fe are not distinguished by electron microprobe, so total Fe is reported as Fe(III) or Fe(II), depending on the expected Fe oxidation state for the mineral. Measurements can also be affected by areas of the grain that have a poor polish or holes in the section. Note that the ochre rims, which are soft and fragile relative to the limestone grains, tend to crack during the grinding and polishing process. Complete rims are not preserved.

Zoning patterns across armored grains (Fig. 7) show that cores are homogeneous, composed of nearly pure calcite. Magnesium contents are minor (<0.5 wt.% MgO) and only trace amounts of other cations are detected. A gypsum rind separates the limestone from the outermost Fe ochre armor.

Patterns of Al distributions across armored grains are complex. The highest Al concentrations observed, up to 8.8 wt.% Al_2O_3, are for transition points between limestone and gypsum, or between gypsum and ochre armor. However, point analyses on flat ochre rim areas commonly contain a few weight percent alumina. SEM spectra (Fig. 6) and electron microprobe maps (Fig. 8) of armored grains show Al enrichment near the inner margins of the ochre armors. In some cases, Al exceeds Fe. This suggests that an Al oxyhydroxide or hydroxysulfate phase may precipitate out before the Fe(III) phase. When the pH of acidic drainage increases (by reaction with carbonate minerals or by mixing with near-neutral dilute waters) to values above about 5,

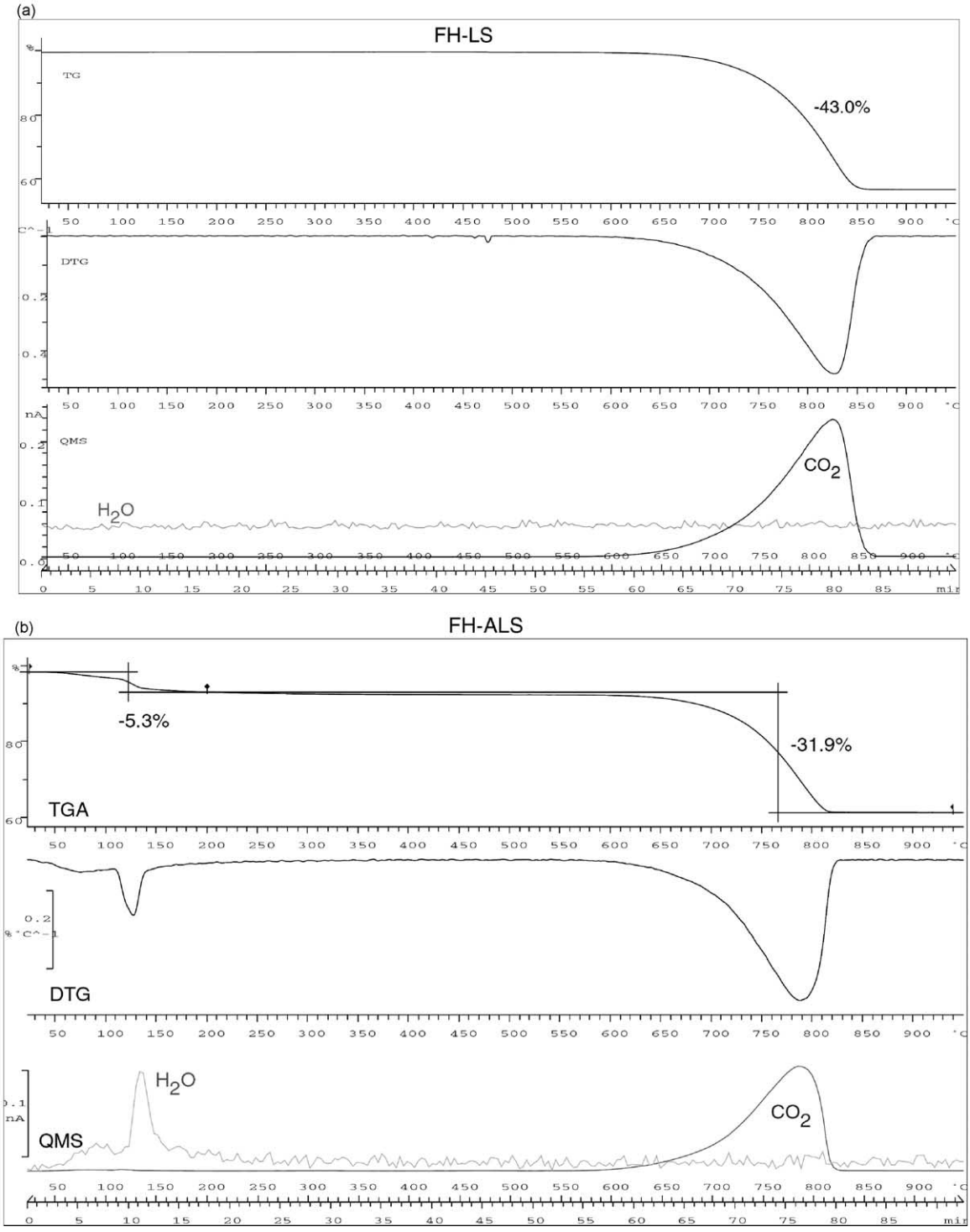

Fig. 3. Thermogravimetric analysis. TGA, mass loss on heating as a function of temperature. DTG, First derivative of mass loss curve. QMS, Quadrupole mass spectrometer data for masses 18 (H_2O) and 44 (CO_2). Samples were heated from 22 to 950 °C at a rate of 10 °C/min in an Ar atmosphere. (a) Limestone feed material sample FH-LS (23.5 mg starting sample mass); (b) armored limestone sample FH-ALS (15.8 mg starting sample mass).

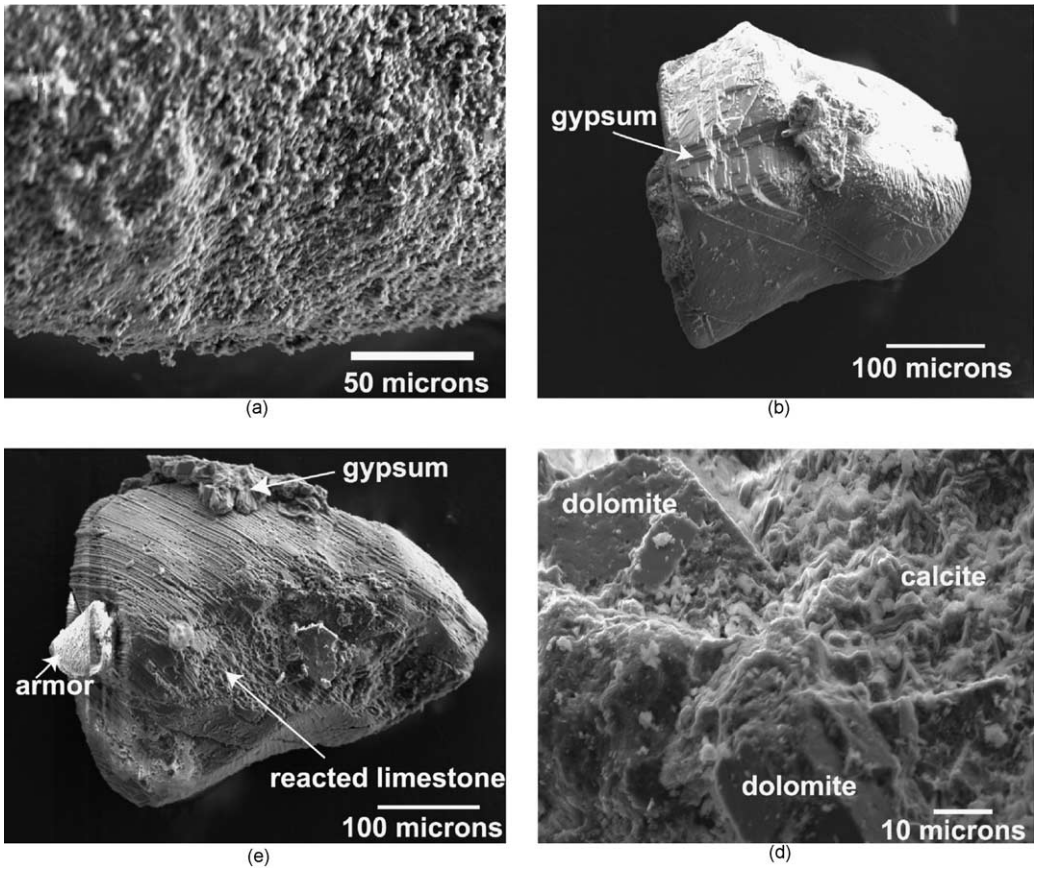

Fig. 4. SEM secondary-electron images of limestone surfaces: (a) raw limestone sand; (b) well-developed gypsum coating on a rounded limestone grain from the 48-h armoring experiment. Armor coating removed by sieving. (c) Reactor limestone grain with a patch of gypsum and armor coating. Note the striations and surface relief developed on the rounded limestone grain. (d) Refractory dolomite (smooth) and etched calcite in reactor limestone.

white precipitates of amorphous or microcrystalline $Al(OH)_3$, or Al hydroxysulfate minerals such as hydrobasaluminite $[Al_4(OH)_{10}(SO4)\cdot 15H_2O]$ or basaluminite $[Al_4(OH)_{10}(SO4)\cdot 4H_2O]$ form spontaneously (Nordstrom and Alpers, 1999; Bigham and Nordstrom, 2000). All of these minerals are white, clay-like, and amorphous to poorly crystalline. In traverses across armored limestone grains in sample FH-ALS, spikes in Al concentrations occur where Ca drops off abruptly at the edge of the limestone. The maximum Al_2O_3 content observed in the microprobe point analyses is about 9 wt.%. Ideal hydrobasaluminite is Fe-free and has 31.7 wt.% Al_2O_3, 55.9 wt.% H_2O, and 12.4 wt.% SO_3 (Bigham and Nordstrom, 2000). X-ray mapping of armored grains (Fig. 8) shows that discrete Al-rich areas develop between partially dissolved calcite cores and outermost Fe-rich rims. Manganese concentrations in armor are near detection limits (about 400 ppm) and no trends in Mn enrichment are observed.

The ochre armor material (Table 4) is Fe-rich and incorporates S (5–6 wt.% SO_3). Variable concentrations of Al, Si and Ca are detected in all of the analyses. Zinc concentrations are at or near the detection limit (0.1–0.2 wt.% ZnO). Compared to natural AMD precipitates described in the literature, the armor material is Ca-rich, but otherwise similar. The reddish-brown color is more typical of a ferrihydrite-like ($Fe_5HO_8\cdot 4H_2O$) phase than of schwertmannite ($Fe_8O_8(SO_4)(OH)_6$, which is yellow. The average molar Fe/S ratio based on microprobe data for the armor is 12.8 (Table 4); this ratio is intermediate between reported molar Fe/S ratios for schwertmannite (<6) and ferrihydrite (>30). Upon controlled heating, a 15.8 mg sample of armored limestone (Fig. 3b) lost 5.3% of its starting mass at 130 °C due to water loss and another 31% due to CO_2 (and SO_2) at 750 to 800 °C. The low temperature water loss reflects dehydration of gypsum and Fe- and Al- precipitates, all of which lose water between 100 and 300 °C. The poorly crystalline Fe-ochre minerals are all metastable with respect to goethite; goethite loses water at higher temperatures (>300 °C). The water loss is not present in the TGA run on unaltered limestone feed material (Fig. 3a).

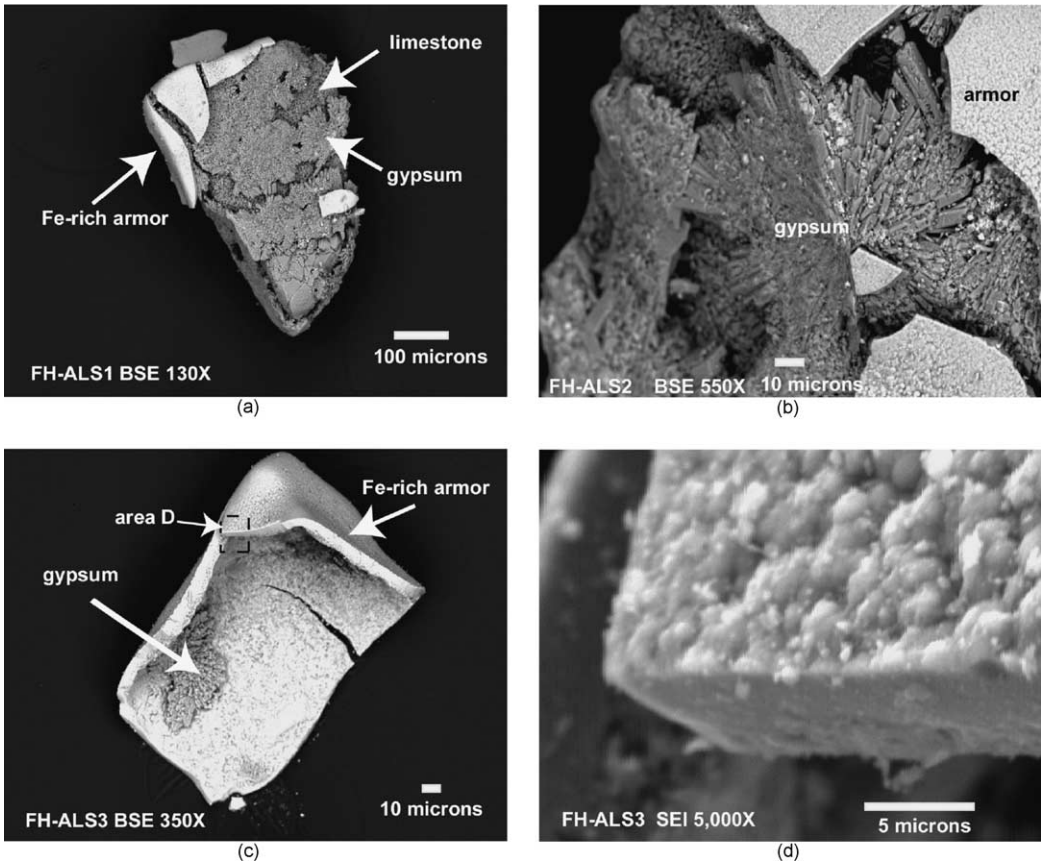

Fig. 5. SEM images of armored limestone: (a) partly armored grain showing gypsum coating on limestone surface; (b) close-up view showing well-developed sprays of gypsum crystals; (c) armor coating broken off limestone core. Note patch of gypsum adhering to inner armor lining. (d) High magnification image of outer armor showing rounded, colloidal-size particles.

5.3. Reactor limestone

Residual grains sampled from the Friendship Hill reactor are heterogeneous. Much of the limestone is gray; however, a distribution of red-colored flakes was visually apparent (Fig. 1c) and some grains are completely armored. Modal analysis showed that 59 vol.% of the grains are not armored, 33 vol.% are almost completely armored, and 8 vol.% are partially armored. Bulk concentrations of Al_2O_3 and Fe_2O_3 for the reactor sample are elevated compared to raw limestone; however, the Fe and SO_4 contents are much lower than those observed for the armored sample (Table 2). The CaO content was also lower than that of raw limestone, indicating calcite dissolution and dilution by precipitated phases, but in this case the limestone was still active in acid neutralization based on plant observations before removal. A BET surface area analysis with N_2 measured 11.8 m^2/g, about 40 times as great as the raw limestone. This suggests that the reactor limestone had developed a porous product layer and/or that dissolution had occurred in an existing pore structure, and had widened or expanded that structure. Most of the reactor limestone grains are white to pale gray in color and are rounded relative to the limestone sand feed material (compare Fig. 1a and c). These represent limestone added as feed material that did not undergo significant dissolution before the system was shut down and the sample was removed. The unarmored grains form the largest particles in the reactor limestone sample, typically > 0.5 mm in diameter. The armored grains are typically small (<0.5 mm in diameter), rounded, and represent an accumulation of material that probably had a much longer residence time in the reactor. The cores of the armored grains are refractory minerals that occur as inclusions in the limestone. Although the limestone is relatively pure, the refractory minerals accumulate from the thousands of kilograms of limestone feed material dissolved in the pulsed limestone bed reactor over the 3-month operation period. Pyrite probably tends to sink and settle near the bottom of the fluidized bed in spite of the pulsing action in the reactor due to its high specific gravity.

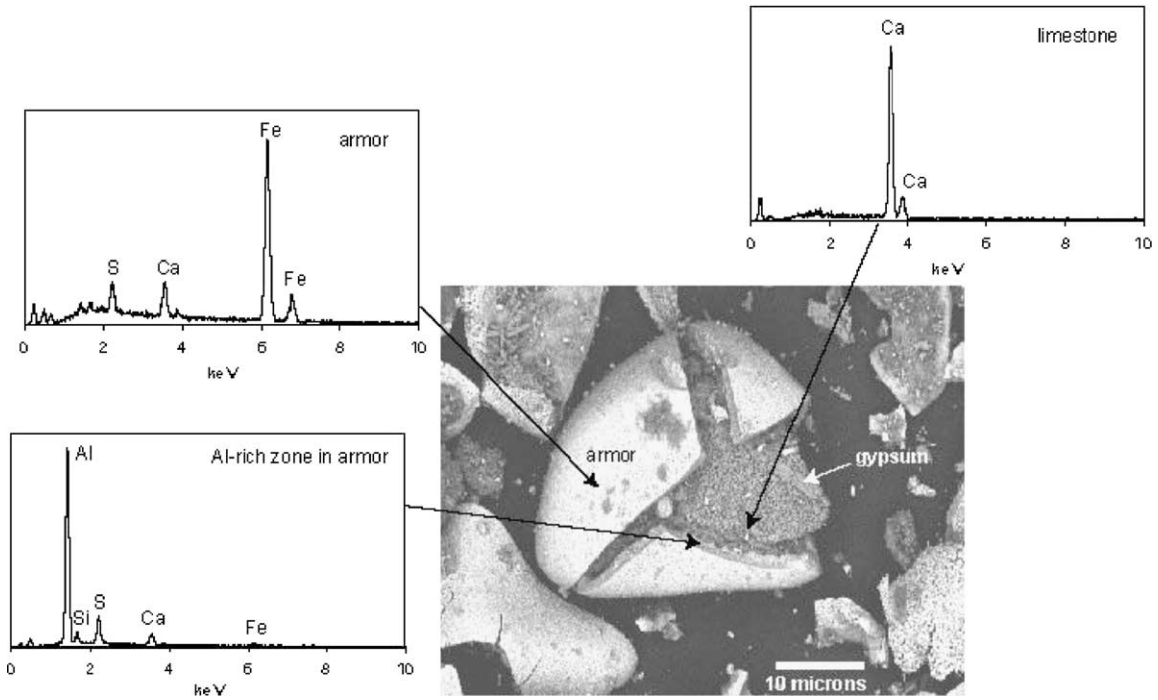

Fig. 6. EDS spectra for armored limestone. The interior of the armor shell is Al-rich relative to the Fe- and S-rich outermost material.

Table 4
Electron microprobe data for ochre rims (this study) compared with chemical data for natural AMD precipitates

	Armored limestone		Reactor limestone		Natural precipitates from AMD streams				
	$n=13$		$n=24$						
	Avg	S.D.	Avg	S.D.	PY4[a]	Ohio[b]	P1974-6[c]	TJS6[d]	PI3[e]
Fe_2O_3	71.3	6.7	42.6	7.6	62.6	61.3- 4.7	67	73.4	67.3
SO_3	5.60	0.32	4.91	1.31	12.7	11.5- 2.9	3.99	1.13	14.7
Al_2O_3	3.31	1.30	18.93	7.85	–	–	5.53	–	–
CuO	0.07	0.09	0.03	0.05	–	–	–	–	–
ZnO	0.13	0.14	0.06	0.08	–	–	–	–	–
MnO	0.02	0.03	0.02	0.02	–	–	–	–	–
MgO	0.07	0.02	0.05	0.03	–	–	0.14	0.02	0.01
CaO	5.41	0.24	1.95	0.41	–	–	0.91	0.33	0.02
K_2O	0.02	0.02	0.03	0.02	–	–	0.04	1.84	0.01
Na_2O	0.11	0.03	0.03	0.02	–	–	0.02	0.21	0.1
SiO_2	1.38	0.18	5.69	3.42	–	–	3.43	3.92	0.08
H_2O	–		–		23.1	18.1- 0.3	16.4	13.4	20.7
Total	87.4		74.34		98.4	91- 98	97.5	96.3	103.1
Fe/S (molar)	12.8		8.7		4.9	4.7- 5.4	36.9	348	4.6

[a] Type specimen of natural schwertmannite from Finnish mine drainage (Bigham et al., 1994).
[b] Natural schwertmannites from Ohio coal mine drainage (Bigham et al., 1990).
[c] Natural precipitate (ferrihydrite and schwertmannite) from Korean coal mine drainage (Yu et al., 1999).
[d] Natural ferrihydrite from Korean coal mine drainage (Yu et al., 1999).
[e] Natural schwertmannite from Korean coal mine drainage (Yu et al., 1999).

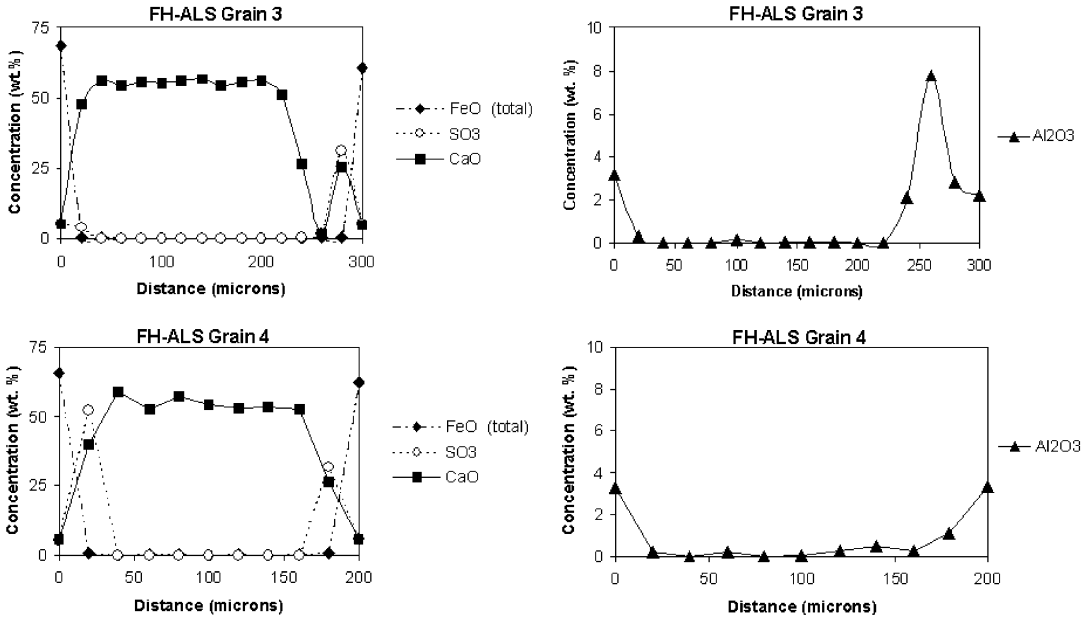

Fig. 7. Electron microprobe point analysis traverses across two armored limestone grains. Traverses start on the Fe-rich armored rim and step across the grain in 20-μm increments, passing through the unaltered limestone core. Note the gypsum rind (elevated CaO and SO_3) at the edge of the limestone core. Alumina increases at the edge of the grains.

Microscopic examination of rounded limestone grain surfaces shows that surfaces are pitted and scoured (Fig. 4c). Gypsum is observed by SEM (Fig. 4c) on a few grains, but is not apparent in the XRD pattern. Armored coatings up to 100 μm thick form on dolomite, pyrite, and on a K–Al–Si–Mg–Fe silicate mineral (probably a mica). Dolomite is less reactive than calcite in acidic solutions and persists longer in the treatment system. The higher concentrations of MgO and SiO_2 in the bulk analysis of reactor limestone (Table 2) reflect the more refractory dolomite, quartz, and other silicate minerals that accumulate. Relative to the armored limestone from the constant flow experiment, the armor on the reactor limestone incorporates more Al and Si and less Fe and Ca on average (Table 4). The Al-rich "spikes" in the inner part of the armor rim observed in the armored limestone are also present in the reactor limestone (Figs. 9 and 10). Within the standard deviation of the analyzed grains, S concentrations of armor from both experiments overlap. Although S was below detection limits in the bulk analysis of raw limestone sand (Table 2), pyrite is observed in polished grain mounts of the material. In the reactor sample, some calcite grains are completely reacted away and the armor is in direct contact with dolomitic limestone (Fig. 10a) or pyrite (Fig. 10b). Note that the armor coatings on the reactor limestone grains (Fig. 10) are much thicker than those that developed in the 48-h experiment. The Al-enrichment zone forms in the interior part of the armor in samples from both experiments. Iron- and Al-zoning patterns in the armor are similar regardless of the mineral present at the core (Fig. 10).

6. Discussion

Numerous field and laboratory studies show that the particular solid phase that forms in a given environment reflects the master variable, pH, as well as dissolved Ca, SO_4, Fe, and Al concentrations. Schwertmannite typically precipitates over a pH range of 2.5–4.5; Al oxyhydroxide and hydroxysulfate white slime precipitates are typically encountered in the pH range 4.5–5.5, and at higher pH (6–8), ferrihydrite is the common ochreous precipitate (Bigham, 1994). The pH ranges represented by the influent and the treated waters overlap these ranges. In natural streams, because of the gradient in pH, the Al- and Fe- precipitates are found spatially separated and Fe-Al coprecipitation is not observed (Bigham and Nordstrom, 2000).

The armor from the 48-h experiment consists of a series of more or less continuous layers: calcite core, inner gypsum rind, thin Al-rich layer, and outermost Fe hydroxysulfate. SEM and microprobe data show that Al-rich areas in the armored grains tend to be Fe- and S-poor, and occur in the inner part of the armor rim near the calcite core (Figs. 6–8). The sequence of deposition of the different armor layers appears to be related to the distance from the limestone surface. One

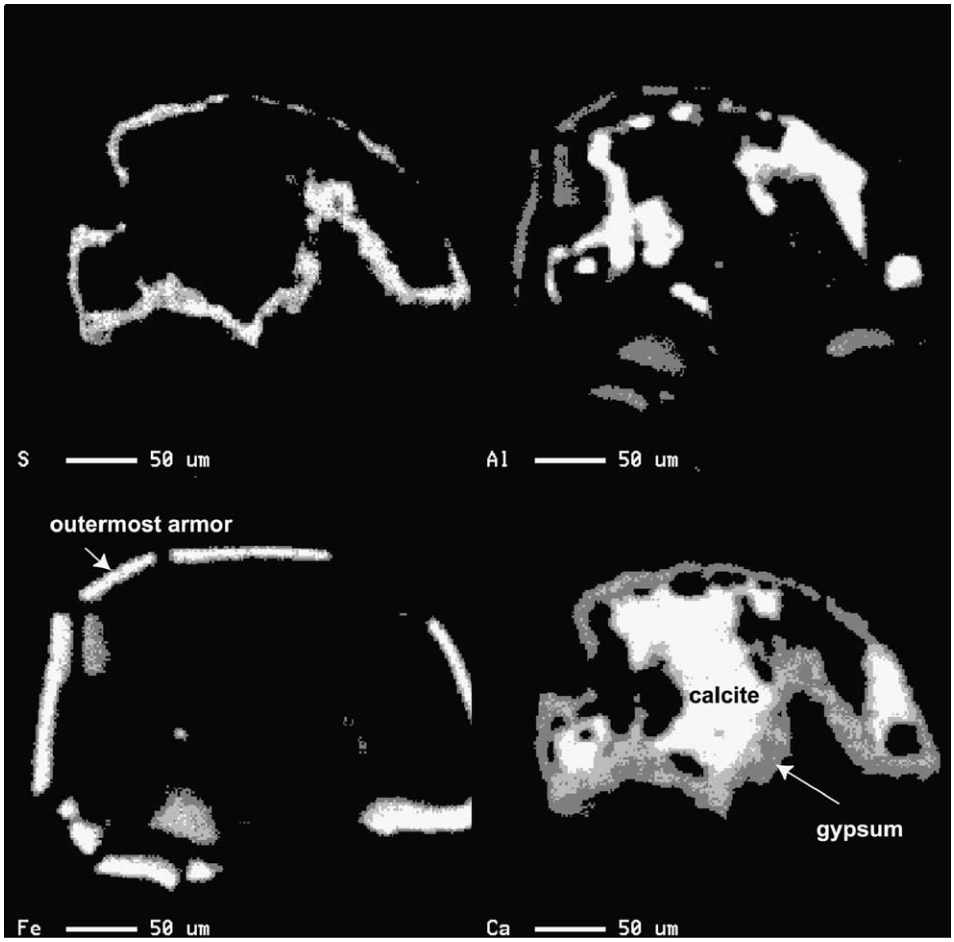

Fig. 8. Map of element distributions across a partially dissolved, armored limestone grain after 48 h of exposure to Friendship Hill AMD. White represents the highest concentration of the element in the field of view. The calcite core is deeply embayed and surrounded by a layer of gypsum (Ca and S). An Al-rich zone forms between the gypsum and the outermost Fe armor.

would expect a gradient in pH, from the bulk value in solution, to an elevated value near the dissolving limestone surface. This explains the occurrence of an Al phase near the limestone surface where pH is likely to reach a value of 5 or higher during the early stages of the experiment. The pH would also be elevated above the bulk value in near-surface calcite macropores, which would cause precipitation of aluminous materials in those areas, as suggested by the Al map of armored limestone (Fig. 8). At lower pH, Al mineral phases are not stable. At a pH of about 3.5, the Fe(III) hydroxysulfate and oxyhydroxides should precipitate. This condition is most likely to be attained further from the reacting limestone surface, which is where these phases were found. Cravotta and Trahan (1999) described spatial zoning when they analyzed ochre crusts developed on limestone slabs immersed at AMD inflows and along oxic limestone drains. In their study, experiments ran for 5–12 months. Molar Al/Fe in armor tended to increase with increasing pH, which correlated with increasing distance from the inflow point along the drain.

The formation of gypsum depends on local dissolved Ca concentrations. Gypsum saturation is achieved in the pulsed limestone bed reactor because gypsum is identified in the ochre that accumulates in the post-treatment settling ponds. As limestone dissolves, Ca^{2+} and carbonate ions diffuse through the mineral–water interface. Therefore, the highest dissolved Ca concentrations will be closest to the dissolving limestone surface, which is where gypsum is observed in the samples. The occurrence of gypsum forming in limestone drains is probably widespread, but may be underreported because of a lack of mineralogical studies. The authors have identified gypsum coatings on a limestone drain armoring with white aluminous precipitates at the Hegins Run coal mine drainage treatment site in Pennsylvania (Hammarstrom, unpublished data). Cravotta

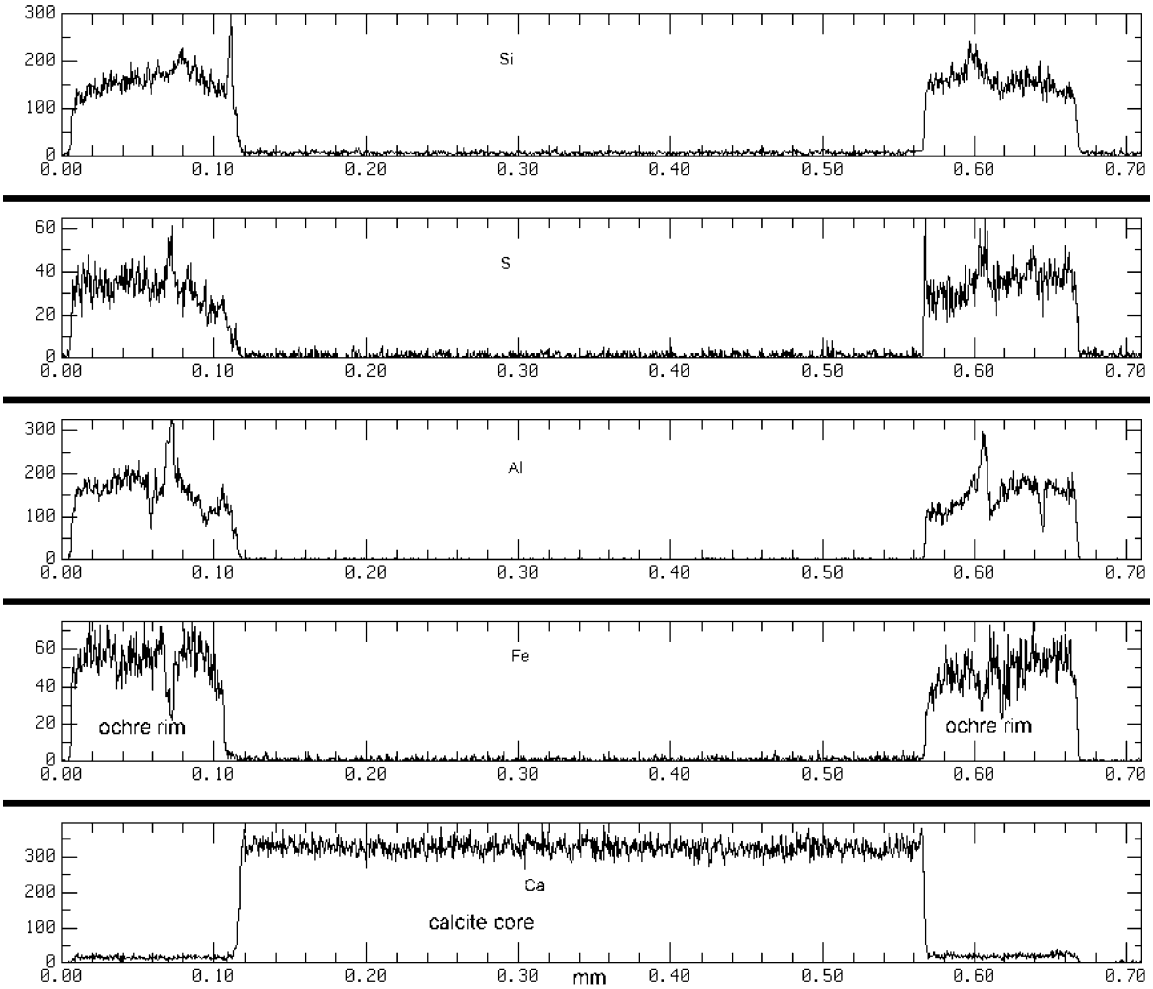

Fig. 9. Traverse across an armored calcite grain in the reactor limestone. Plots show counts as a function of distance. Note the absence of gypsum and the spikes in Al and S concentrations at a distance of 0.07 mm into the grain and again at 0.61 mm on the opposite side of the calcite core.

and Trahan (1999) found that AMD waters flowing through oxic limestone drains remained undersaturated with respect to calcite and gypsum despite increases in alkalinity and pH. Therefore, calcite continued to dissolve rather than precipitate during operation of the drain and gypsum did not form. Their influent waters contained significantly less dissolved SO_4 (130–300 mg/l SO_4) than the Friendship Hill AMD (2200 mg/l SO_4). The dissolved SO_4 concentration of many AMD waters may be too low for gypsum saturation to occur.

The armor coating that develops on residual refractory grains such as pyrite or dolomitic limestone (Figs. 9 and 10) may have formed on the grains when calcite was still present, or by continued slow dissolution of limestone after development of an armor coating. The refractory grains would tend to remain in the reactor because of their greater specific gravity, and must have been in the reactor for an extended period of time for complete dissolution of the calcite matrix. However, gypsum would also be expected to precipitate under these conditions, and no gypsum is apparent in microprobe traverses across core–armor interfaces on armored refractory mineral grains. The dynamic environment in the pulsed bed enhanced scouring and spalling of gypsum and armor, and could have removed gypsum deposits, but it seems unlikely that all of the gypsum could be removed and still leave the Al- and Fe-rich phases intact. Another possible explanation for the observed results is that the refractory grains served as a seed surface for continuous precipitate growth. Due to mixing of treated waters with acidic influent, oversaturation of pH-dependant phases such as Fe and Al oxyhydroxides would be expected to occur. In experiments reacting calcite with Fe(III) perchlorate as a

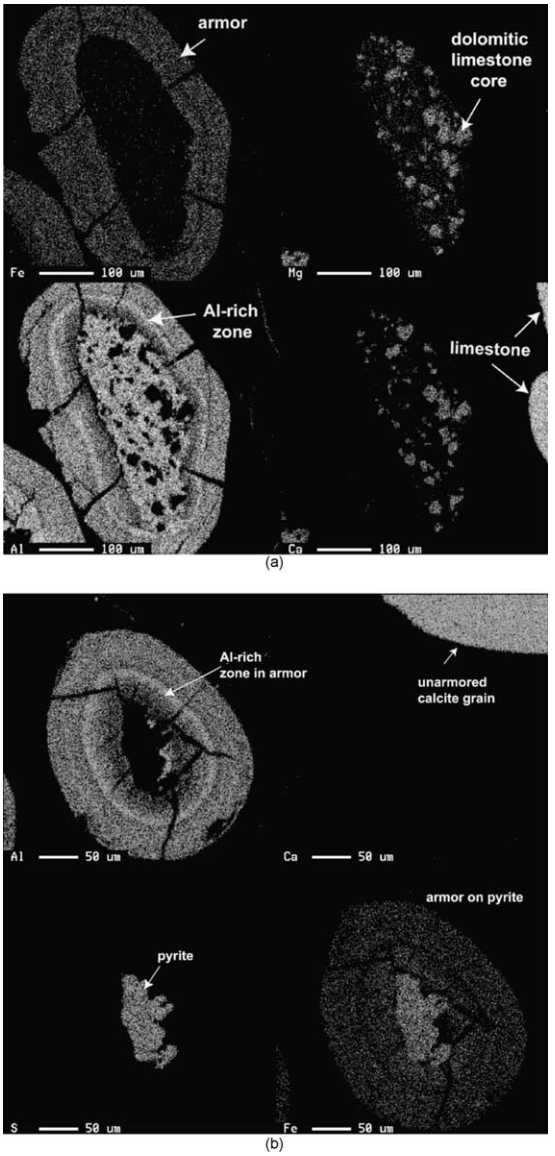

Fig. 10. Maps showing the distribution of elements in refractory grains in reactor limestone: (a) zoned Fe- and Al-rich 50-μm thick armor coating developed on dolomitic limestone. Adjacent calcite-rich limestone grains (see Ca map) are rounded, but show no armor overgrowth. (b) Armored pyrite grain. Note unarmored calcite grain in upper corner of Ca map and lack of any Ca in the area of the armored pyrite grain.

source of Fe^{3+}, Loeppert and Hossner (1984) demonstrated that direct contact with calcite is not necessary for polymerization and precipitation of $Fe(OH)_3$. The Fe and Al oxides would tend to precipitate on solid surfaces in the reactor, including unreactive particles such as armored calcite, and residual pyrite and dolomite. The high density sludge process takes advantage of this tendency for precipitation of metal hydroxide phases onto seed crystals to result in a much more compact precipitate from lime-based AMD neutralization plants (Dempsey and Jeon, 2001). Gypsum would not be expected to form by this mechanism because there would be no Ca^{++} gradient.

Zoning patterns that develop in armors indicate that the composition of the precipitating phase varies in response to changing chemical conditions at the solid/water interface. The overall composition of the armor on the refractory grains in the reactor sample is much more aluminous than the armor that forms in the 48-h experiment; from grain to grain; however, the Al content of the armor is highly variable. This is reflected in the high standard deviations for Fe and Al (Table 4). Nevertheless, Al-enriched zones develop within the relatively thick (50 μm) Fe–Al rinds on the refractory grains. The reactors were recharged with limestone twice weekly during the 3-month period. Aluminium-enriched zones in the armor coating may reflect an abrupt increase in alkalinity following limestone recharge. Once formed, armor coatings may be modified by diffusion depending on concentration gradients and surface complex equilibria.

Armor formation proceeded very quickly under the conditions of the baseline experiment. Within 48 h of exposure to AMD, the gypsum layer formed, a μm-scale Al-rich layer was deposited, and a 10- to 30-μm thick, Fe-rich ochre encapsulated the limestone sand grains. The lack of continuous gypsum rinds and the paucity of armor coatings on residual limestone from the pulsed limestone bed system is probably due to disruption of fresh precipitate surface contacts by elevated CO_2 concentration and scouring of limestone surfaces in the pulsed fluidized bed.

7. Conclusions

Mineralogical characterization of limestone samples documents the chemical and physical processes of limestone use in AMD treatment. The use of CO_2 and pulsed fluidized beds to enhance limestone reactivity in AMD treatment systems retarded limestone armoring in acidic AMD with elevated concentrations of Fe, Al, and dissolved SO_4. In the absence of CO_2 and pulsing, limestone grains were coated with a layer of gypsum crystals and become almost completely encapsulated in a 10- to 30-μm thick Fe–Al hydroxysulfate armor within 48 h. Although the ochre armor readily flakes off upon drying, the gypsum coating under the armor appears to be more stable and prevents or retards further limestone dissolution. With CO_2 and pulsing in longer-term operation of the reactor, limestone grains completely dissolve leaving a residue of armored refractory minerals and rounded to partially reacted limestone grains. Partially dissolved calcite-rich limestone grains develop

etched surfaces in the reactor. The residual refractory mineral phases include dolomite, mica, quartz and pyrite that are present in minor amounts as inclusions in the relatively pure limestone sand feed material. The modal abundance of armored grains from the reactor after 3 months of operation with biweekly limestone replenishment is about 30% armored grains. The physical and chemical effects of CO_2 and pulsing in the fluidized bed reactor effectively prevent armoring by gypsum and metal hydroxysulfate precipitates and appear to maximize the ability of limestone to produce alkalinity to treat AMD. Although the data apply to a particular AMD composition, Friendship Hill AMD is relatively acidic and contains elevated concentrations of dissolved Fe, Al, and SO_4. Lower acidities and metal contents would be expected to present less potential for armoring. The use of the new pulsed limestone bed technology to enhance limestone dissolution holds promise for treating many other coal mine AMD situations where metal and SO_4 concentrations exceed the optimal parameters for use of passive treatment systems alone.

Acknowledgements

The authors thank Nadine Piatak of the USGS, Reston, VA for laboratory assistance. USGS colleagues Robert R. Seal, II and I-Ming Chou provided reviews of early drafts of this manuscript; comments by two anonymous reviewers provided additional insights. Barnaby Watten provided helpful comments at all stages of this study. Demonstration of the pulsed limestone bed process at Friendship Hill was funded by the National Resources Preservation Program (NRPP), a collaborative research program between the Biological Resources Discipline of USGS and the National Park Service.

References

Berkheiser Jr., S.W., 1985. Warner Company's Bellefonte operation. Pennsylvania Geol. 16 (2), 6–10.

Bigham, J.M., 1994, Mineralogy of ochre deposits formed by sulfide oxidation. In: Jambor, J.L., Blowes, D.W. (Eds.), The Environmental Geochemistry of Sulfide Mine-wastes. Short Course Handbook, Vol. 22. Mineralogical Association of Canada, pp. 103–132.

Bigham, J.M., Nordstrom, D.K., 2000. Iron and aluminum hydroxysulfates from acid sulfate waters. In: Alpers, C.N., Jambor, J.L., Nordstrom, D.K. (Eds.), Sulfate Minerals, Reviews in Mineralogy and Geochemistry, Vol. 40. Mineralogical Society of America, Washington, DC, pp. 351–403. (Chapter 7).

Bigham, J.M., Schwertmann, U., Carlson, L., Murad, E., 1990. A poorly crystallized oxyhydroxysulfate of iron formed by bacterial oxidation of Fe(II) in acid mine waters. Geochim. Cosmochim. Acta 54, 2743–2758.

Bigham, J.M., Carlson, L., Murad, E., 1994. Schwertmannite, a new iron oxyhydroxysulfate from Pyhasalmi, Finland, and other localities. Min. Mag. 58, 641–664.

Booth, J., Hong, Q., Crompton, R.G., Prout, K., Payne, R.M., 1997. Gypsum overgrowths passivate calcite to acid attack. J. Colloid Interface Sci. 192, 207–214.

Cravotta III, C.A., Trahan, M.K., 1999. Limestone drains to increase pH and remove dissolved metals from acidic mine drainage. Appl. Geochem. 14, 581–606.

Deer, W.A., Howie, R.A., Zussman, J., 1967. An Introduction to the Rock-Forming Minerals. Longmans, London.

Dempsey, B.A., Jeon, B., 2001. Characteristics of sludge produced from passive treatment of mine drainage. Geochem. Explor., Environ., Anal. 1, 89–94.

Evangelou, V.P., 1995. Pyrite Oxidation and Its Control. CRC Press, Boca Raton, FL.

Geo-Technical Services, Inc., 1982. Quakake Tunnel Demonstration Project. Limestone Neutralization of Acid Mine Drainage (Project No. SL 135-10). Pennsylvania Department of Environmental Protection, Harrisburg, PA.

Geiger, G.H., Poirier, D.R., 1973. Transport Phenomena in Metallurgy. Addison-Wesley, Reading, MA. p. 97.

Hedin, R.S., Narin, R.W., Kleinmann, R.L.P., 1994. Passive Treatment of Coal Mine Drainage. US Bureau of Mines Information Circular 9389.

ICCD, 2000. Powder Diffraction File Release 2000 Data Sets 1-50 plus 70-88:International Centre for Diffraction Data, Newton Square, PA. Available from <www.icdd.com>.

Leith, S.D., Reddy, M.M., Ramirez, W.F., Heymans, M.J., 1996. Limestone characterization to model damage from acidic precipitation: effect of pore structure on mass transfer. Environ. Sci. Technol. 30, 2202–2210.

Loeppert, R.H., Hossner, L.R., 1984. Reaction of Fe^{2+} and Fe^{3+} with calcite. Clays and Clay Minerals 32 (3), 213–222.

Nordstrom, D.K., Alpers, C.N., 1999. Geochemistry of acid mine water. In: Plumlee, G.S., Logsdon, J.J. (Eds.), The Environmental Geochemistry of Mineral Deposits, Part A. pp. 133–160 (Chapter 6).

Pearson, F.H., McDonnell, A.J., 1975a. Use of crushed limestone to neutralize acid wastes. J. Environ. Eng. Div. of ASCE 101 (EE1), 139–158.

Pearson, F.H., McDonnell, A.J., 1975b. Limestone barriers to neutralize acidic streams. J. Env. Eng. Div. of ASCE 101 (EE3), 425–440.

Phipps, T.T., Fletcher, J.J., Skousen, J.G., 1995. Costs for chemical treatment of AMD. In: Skousen, J.G., Ziemkiewicz, P.F. (Eds.), Acid Mine Drainage Control and Treatment. West Virginia University and the National Mine Lands Reclamation Center, Morgantown, WV, pp. 145–171. (Chapter 17).

Robbins, E.I., Cravotta III, C.A., Savela, C.E., Nord Jr., G.L., 1999. Hydrobiogeochemical interactions in 'anoxic' limestone drains for neutralization of acidic mine drainage. Fuel 78, 259–278.

Rose, A.W., Cravotta, C.A., III. 1998. Geochemistry of coalmine drainage. In: Smith, M.W., Brady, K.B.C. (Eds.), The Prediction and Prevention of Acid Drainage from Surface Coal Mines in Pennsylvania. Pennsylvania Department of Environmental Protection, Harrisburg (Chapter 1).

Sibrell, P.L., Watten, B.J., Friedrich, A.E., Vinci, B.J., 2000. ARD remediation with limestone in a CO_2 pressurized reactor.

In: Proc., 5th Internat. Conf. Acid Rock Drainage, Society for Mining, Metallurgy, and Exploration, Denver, CO, 1017–1026.

Skousen, J., Politan, K., Hilton, T., Meek, A., 1995. Acid mine drainage treatment systems: chemicals and costs. In: Skousen, J.G., Ziemkiewicz, P.F., (Compilers), Acid Mine Drainage—Control and treatment. West Virginia University and the National Mine Land Reclamation Center, Morgantown, WV, pp. 121-129 (Chapter 14).

US Environmental Protection Agency, 2000. National Water Quality Inventory, 1998 Report to Congress (EPA 841-R-00-001). EPA Office of Water, Washington, DC.

Watten, B.J., 1999. Process and Apparatus for Carbon Dioxide Pretreatment and Accelerated Limestone Dissolution for Treatment of Acidified Water (US Patent No. 5,914,046). US Department of Commerce, Washington, DC.

Watzlaf, R.R., Schroeder, K.T., Kairies, C.L., 2000. Long-term performance of anoxic limestone drains. Mine Water Environ. 19, 98–110.

Wentzler, T.H., Aplan, F.F., 1972. Kinetics of limestone dissolution by acid waste waters. In: Rampacek, K. (Ed.), Environmental Control, Proc., 101st AIME Ann. Meeting, pp. 513–524.

Webb, P., Orr, C., 1997. Analytical Methods in Fine Particle Technology. Micromeritics Materials Analysis Laboratory, Norcross, GA.

Wilkins, S.J., Compton, R.G., Taylor, M.A., Viles, H.A., 2001. Channel flow cell studies of the inhibiting action of gypsum on the dissolution kinetics of calcite: a laboratory approach with implications for field monitoring. J. Colloid Interface Sci. 236, 354–361.

Yu, J.Y., Heo, B., Choi, I., Cho, J., Chang, H., 1999. Apparent solubilities of schwertmannite and ferrihydrite in natural stream waters polluted by mine drainage. Geochim. Cosmochim. Acta 63, 3407–3416.

Ziemkiewicz, P.F., Skousen, J.G., Brant, D.L., Sterner, P.L., Lovett, R.J., 1997. Acid mine drainage treatment with armored limestone in open limestone channels. J. Environ. Qual. 26, 1017–1024.